Journal of Alloys and Compounds 822 (2020) 153643

Contents lists available at ScienceDirect

Journal of Alloys and Compounds

journal homepage: http://www.elsevier.com/locate/jalcom

Wetting behavior and reactivity of liquid Si-10Zr alloy in contact with glassy carbon

Donatella Giuranno [a, b, *], Adelajda Polkowska [b], Wojciech Polkowski [b], Rada Novakovic [a]

[a] National Research Council of Italy, Institute of Condensed Matter Chemistry and Technologies for Energy, Via De Marini 6, 16149, Genova, Italy
[b] Łukasiewicz Research Network, Foundry Research Institute, Zakopiańska 73 Str., 30-418, Krakow, Poland

ARTICLE INFO

Article history:
Received 10 September 2019
Received in revised form
2 December 2019
Accepted 1 January 2020
Available online 7 January 2020

Keywords:
Silicon carbide
Metal matrix composites
Liquid Si-based alloys
Refractory materials

ABSTRACT

In designing advanced refractory composites for highly demanding applications, reactive infiltration of liquid Si-enriched Si-Zr alloys into C-or SiC-based preforms may be a viable cost-less manufacturing process.

In such cases, in view to optimize liquid assisted processes such as reactive infiltration, fundamental investigations of the interfacial phenomena occurring when the liquid Si-Zr alloys are in contact with C and SiC substrates, are key steps.

For this reason, aiming to "mimic" the conventional operating conditions imposed within a reactive infiltration process, the contact heating sessile drop method was applied to perform a basic study concerning the interaction phenomena taking place at the interface of Si-10% at Zr alloy/Glassy Carbon substrate under an Ar atmosphere. Specifically, the contact angle values as a function of time were measured in the temperature range of 1354–1500 °C.

The final contact angle values decreased slightly with an increase in temperature.Moreover, at T = 1450 °C, the contact angle increased over a larger time interval before reaching its final value. The kinetics of SiC crystal growth at the interface and the related processing parameters such as temperature and time were carefully analysed. The growth of SiC crystals and their packaging phenomenon are time and temperature-dependent phenomena.

1. Introduction

Ceramic matrix and refractory metal matrix composites reinforced by high strength continuous ceramic fibers, emerge as ideal candidates in several high temperature applications because of their superior high temperature strength, low density and improved damage tolerance [1–4]. In particular, metal matrix composites and SiC-based composites reinforced by C and SiC fibers, are promising materials for highly demanding engineering and industrial applications such as heat shields and thermal barriers, structural components for nuclear reactors and re-entry space vehicles, highly performant brake discs and even high temperature heat exchanger tubes owing to their high strength and improved thermal shock, wear, hardness and corrosion resistance [2,5–8].

In designing refractory materials for nuclear industry, remarkable efforts are currently focused into development of fully dense SiC-based composites and in seeking the suitable method for joining simple shapes to more complex structures, particularly for advanced fission systems and even fusion reactor first wall vessels [7,9–12]. In this context, the materials of interest are "nuclear grade" SiC/SiC_f composites, which consist of high crystalline, near stoichiometric SiC fibers, high crystalline SiC matrix, and C or multilayer C/SiC interphase. Among the possible options under study to densify such materials, the use of a metal phase as a filler for a SiC/SiC_f composite or C_f/SiC, such as the transition metal silicides, emerges as one of the most promising densifying processes [9–12].

The last mentioned are hard materials, chemically inert, and exhibit high electrical and thermal stability [13]. Moreover, their resistance to oxidation, particularly at high temperatures, may be improved by the formation of a stable passivating oxide scale layer.

Among silicides, zirconium silicide is the most promising candidate material for the nuclear industry. Indeed, it worth to be

* Corresponding author. National Research Council of Italy, Institute of Condensed Matter Chemistry and Technologies for Energy, Via De Marini 6, 16149, Genova, Italy.
E-mail addresses: donatella.giuranno@ge.icmate.cnr.it (D. Giuranno), adelajda.polkowska@iod.krakow.pl (A. Polkowska), wojciech.polkowski@iod.krakow.pl (W. Polkowski), rada.novakovic@ge.icmate.cnr.it (R. Novakovic).

https://doi.org/10.1016/j.jallcom.2020.153643

pointed out that Zr, Zr-based alloys and Zr combined with Si are commonly used as cladding materials for nuclear reactors because of their ultra-high neutron capture cross sections consequently improving the reactor performance and preventing irradiation damage to outer structural compounds [14,15]. Concerning Si-Zr alloys, the Si-Zr phase diagram shows a few intermetallic compounds, some of them with a remarkable high melting point [16–18]. Moreover, under high temperature and oxidative/corrosive working conditions, a Zr-silicide compound can naturally evolve into a graded multilayered system of ZrO_2 and SiO_2 sandwich that can potentially provide the necessary protection even in an aggressive ambient [11,19]. For this reason, Si and Zr are used as alloying elements for several Ti-based alloys with aim to improve their oxidation resistance and to significantly increase their mechanical response of "biomaterials" [20]. In addition, the Zr-8.8 at% Si alloy, with small addition of Nb, exhibits excellent biocompatibility and good mechanical properties to be promising candidate, in the context of novel bio-materials, as a valid alternative to the currently used Ti-6Al-4V alloy, as documented by Ref. [21].

As structural materials for applications in extreme environments, it was demonstrated by Ref. [11] that the C/C-ZrC-SiC composites possess outstanding ablation and erosion resistance even at temperatures over T = 1600 °C. Specifically, compared to C/C and C/C-SiC composites, the mass ablation rates of C/C-ZrC-SiC was more than halved. The C_f/ZrC–SiC composites were fabricated by reactive melt infiltration method using C felt preforms infiltrated by the liquid Si-8.8 at% Zr alloy as a precursor and thermally treated at T = 1800 °C for 1 h by Ref. [22]. On the contrary, a dense C_f/C-SiC-$ZrSi_2$ was obtained by infiltrating a C/C preform with liquid Si-10 at% Zr alloy at a T = 1450 °C for 1 h by Ref. [23]. The composite was then converted to a C/C-ZrC-SiC and its ablation resistance was tested. In order to limit C-dissolution phenomenon occurring within reactive infiltration process, in both cases, the C fibers were previously coated with pyrolytic carbon by chemical vapour deposition process. Moreover, dense SiC/$ZrSi_2$ composites were successfully produced by reactive infiltration of liquid Si-rich alloys of the Si-Zr system into a bi-modal SiC preform [24]. That composite shown an excellent thermal compatibility between the metal phase and SiC reinforcement without any evidence of debonding phenomena or residual stress. In addition, the low CTE value measured on the produced composite, candidates such material for highly demanding applications.

The excellent thermo-mechanical response and corrosion resistance exhibited by the as produced composites, combined with the costless route used for their manufacture, make such materials extremely competitive and marketable. Indeed, it is well known that the reactive infiltration process or even spontaneous infiltration possesses advantages over other conventional and costly sintering and hot-pressing techniques i.e. lower processing temperatures, shorter times and nearly-net shape fabrication capabilities [25,26]. A "compact" microstructure can be effort-less obtained by controlling the process parameters (temperature, total pressure, porosity etc.) and promoting good wetting between the reinforcement and the matrix, which are crucial for self-permeation. Whether the molten metal can spontaneously infiltrate into porous media depends on the contact angle value displayed at the pore walls the between the liquid infiltrating media and the reinforcement, which must be significantly less than 90°. On the other hand, the interfacial phenomena occurring at the metal/ceramics interfaces are not easy to be defined and controlled, since wettability is usually accompanied by concurring phenomena such as diffusion, reaction, etc. In fact, the "spontaneous" infiltration process is frequently accompanied by strong reaction phenomena at the pore walls. For this reason, the knowledge and thus, the control of the overall interfacial phenomena evolving between reinforcements and metal matrix during the fabrication process or even in service, are key issues that should be taken into account in selecting the reactive infiltration as fabrication route or joining technique for composites. Specifically, some interactions may cause interfacial instability and decomposition of the C or SiC fibers, formation and growth of brittle intermetallic compounds, resulting in a decreasing of their overall thermo-mechanical properties.

The knowledge of the thermodynamic and thermophysical properties of the liquid phase, such as surface properties (surface tension and surface segregation), density, viscosity [27–29] and, in parallel, of the wetting characteristics and reactivity concerning reacting phases, as pointed out by Refs. [30–32] are essential to be used as input for optimization of the infiltration process [33–35].

To our best knowledge, there are few basic studies on liquid Si-enriched Si-Zr alloys concerning calculations [36] and measurements [37] of the surface tension and fundamental wetting characteristics determination of Si-8 at% Zr alloy onto (GC) glassy carbon and SiC substrates as a function of the operating conditions (temperature, atmosphere) [38].

Aiming to cover the lack of literature data, a systematic investigation on the wetting characteristics and reactivity of Si-10 at% Zr alloy/GC system (from now Si-10Zr alloy/GC) as a function of temperature and time was performed by contact heating sessile drop method and the more relevant results are presented and discussed in this paper. In particular, the wetting experiments on the Si-10Zr alloy/GC system were carried out at the alloy melting point (detected at T = 1354 °C) as well as and at T = 1400, 1450 and 1500 °C in order to cover the entire range of temperatures conventionally used for industrial processes. Moreover, in order to analyse the kinetics of the reactive layer growth (i.e. SiC) at the alloy/GC interface at T = 1450 °C, the wettability was investigated as a function of time. To prevent evaporation and oxidation phenomena, the wetting experiments were performed under an Ar atmosphere. The microstructure characterization of the interfaces by Optical and Scanning Electron Microscopy combined with an Energy Dispersive X-Ray analyser was done.

The influence of experimental conditions on the wettability and spreading kinetics of the Si-10Zr alloy in contact with GC in terms of the interfacial reactions, formation and growth of reaction layer and subsequent microstructural evolution was analysed. The present research provide new findings helpful to define the key parameters governing the reactive infiltration process and its optimization in view of design and microstructure tailoring of C/C-SiC-$ZrSi_2$ and C/C-ZrC-SiC composites.

2. Wetting tests: Experimental details

2.1. Materials and sample preparation

Glassy Carbon (GC) provided by Alfa-Aesar was selected as C-substrate material and used with as received surface conditions. A surface roughness of Ra ≈ 20 nm on a GC area of 3 × 3 mm^2 was measured by an optical confocal-interferometric profilometer (Sensofar S-neox).

The Si-10Zr alloy samples were prepared from high purity Si and Zr (99.98%-Goodfellow®) by mixing pure metals of nominal compositions, mechanically cleaned and the weighted pieces were melted by an arc melting furnace under an atmosphere of Ar (N60, O_2 < 0.1 ppm). Previously, a Zr drop was melted and the residual oxygen content inside the chamber was reduced. To ensure the homogeneity of the alloy composition, each Si-Zr sample (0,05 g) was melted 3 times. By checking the final weight of the alloy samples, no evidences of evaporation or material loss were found. The microstructure and composition of as produced Si-Zr alloys at

the cross-sectioned sample were checked by SEM/EDS.

As it is shown in Fig. 1, the typical eutectic microstructure of the bulk alloy was detected. EDS analysis indicates the eutectic composition with Zr-content varying from 8.15 to 9 at%. On the contrary, some $ZrSi_2$ precipitates were detected embedded into the eutectic matrix at the bottom and as a layered phase segregated at the surface of the solidified drop. The presence of $ZrSi_2$ precipitates dispersed into the eutectic matrix is due to an excess of Zr-content in the alloy with respect to the eutectic composition.

Prior to the experiments, the Si-10Zr alloy sample and GC substrate were weighted, rinsed in an ultrasonic bath and dried with compressed air.

2.2. Contact heating sessile drop experiments: device and procedure

At room temperature, the assembled Si-10Zr alloy/GC substrate couple was placed on a graphite sample holder, located at the central part of the heater and leveled at the horizontal plane, as shown in Fig. 2.

In order to remove any contaminant from the experimental environment, the device was degassed under a vacuum ($P_{tot} < 10^{-6}$ mbar) for 2 h.

The alloy sample/substrate couple was heated by an 800 kHz high frequency generator coupled to a graphite susceptor (Fig. 2a). The presence of graphite as heating element provides an atmosphere with reduced oxygen content ($PO_2 << 10^{-8}$ mbar).

In order to avoid evaporation phenomena, typically occurring during measurements of liquid Si-based alloys [30,31,38], mainly over their melting temperature, the wetting experiments were performed under an Ar atmosphere ($O_2 < 0.1$ ppm) by following the procedure described elsewhere [30,31].

During the wetting experiments, as shown in Fig. 2b, the temperature was in real time monitored by a pyrometer (Minolta-CYCLOPS52), previously calibrated by detecting the melting temperature of high purity metals (Sn, Al, Au, Cu, Si and Ni).

Except for the wetting test performed at T = 1354 °C (detected alloy melting point), the wetting experiments were performed under the isothermal conditions with a heating rate of 10 °C/s. The selected temperature was kept constant for around 15 min, then the sample was “quenched” (cooling rate 20 °C/s) to “freeze” the formed reaction products and developed interface microstructures.

The evolution of contact angles values over time was monitored in real-time and recorded (10 frames/sec) by a high resolution CCD-camera connected to a computer (Fig. 2a).

Every single frame was processed by an image analysis software ad hoc-developed (ASTRAVIEW®) [39] allowing automatic acquisition of the contact angle values and drop geometric variables (R-base radius and H-drop height). By analyzing the experimental method used and all the factors that can affect measured contact angle value, the accuracy of the data obtained is estimated to be around ±2° [40].

2.3. Surface and microstructural characterization

After the wetting tests, all the Si-10Zr alloy/GC samples were embedded in epoxy-resin, cross-sectioned and metallographically polished and prepared for the microstructural characterization. The microstructural evolution was analysed on both the top and the cross-section of solidified drop by an Optical Microscope (ZEISS) and a Scanning Electron Microscopy (SEM) equipped with an energy dispersive X-Ray detectors (EDS).

3. Results

3.1. Wettability tests by the contact-heating sessile drop method as a function of temperature

The wetting behavior of the liquid Si-10Zr alloy in contact with GC observed at the alloy melting temperature (T = 1354 °C) is shown in Fig. 3. The variations of the contact angle values as a function of time and the sequence of images acquired within the first 100 s of the experiment (Fig. 3b–c), indicate the wetting kinetics on GC with an irregular behavior most probably caused by the progressively melting alloy drop. In spite of the fact that for t = 30 s the alloy was only partially melted, the Si-10Zr/GC interface was crossing the threshold contact angle value of θ = 90° and the transition between no-wetting to wetting behavior was observed. The complete melting of the alloy drop took around 50 s resulting in the contact angle value around θ = 75°. A further decrease of the contact angle value of 19° occurred within the next 15 s, then it was

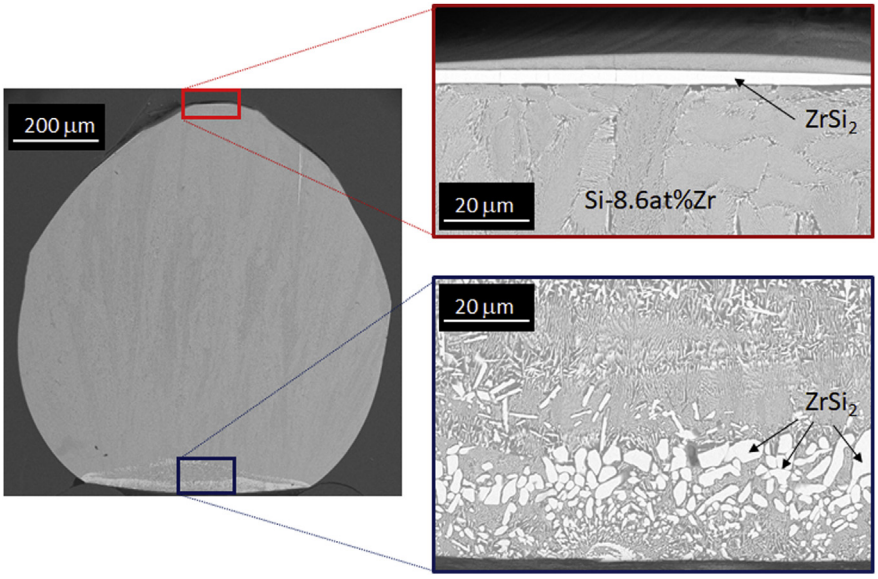

Fig. 1. BSE/EDS images of the cross-sectioned as-produced Si-10Zr alloy sample at two magnifications.

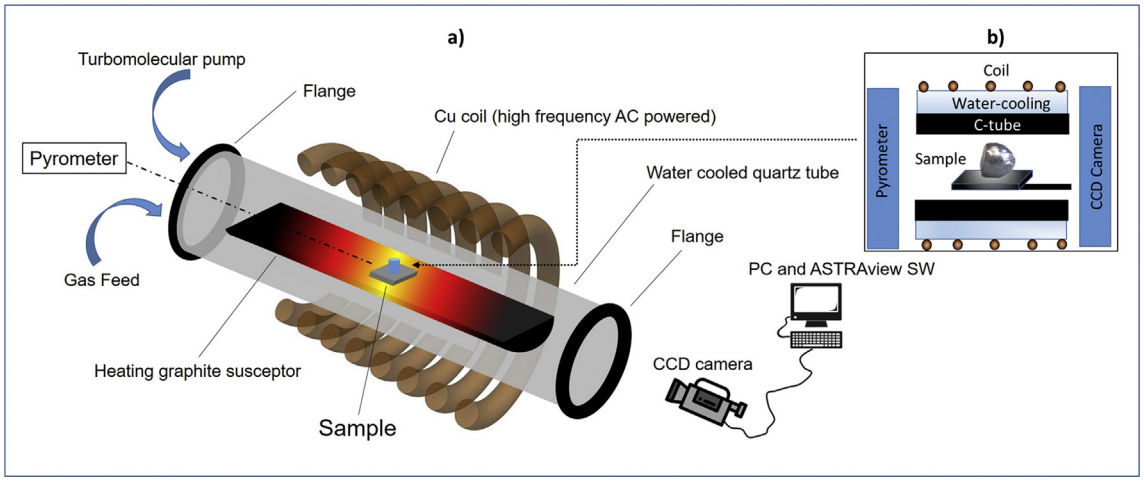

Fig. 2. Schematic layout of the a) experimental set-up used and b) Si-10Zr/GC couple assembled for the wetting experiments.

limited to 4° during 60 s, reaching the value of 51°. After t = 450 s, a weak increase of the contact angle value ($\theta = 52°$) was recorded and kept constant until the end of the experiment. At the same time, at the top drop, the solid phase was detected (Fig. 3c).

Fig. 4 shows the wetting kinetics of the Si-10Zr/GC system observed at different temperatures. As it can be seen, by increasing the testing temperature with respect to T = 1354 °C, the achievement of an equilibrium contact angle of liquid Si-10Zr on GC substrate is evidently dependent on temperature. Moreover, by analyzing the spreading kinetics (U_{spr}), without considering the melting at T = 1354 °C, it results that U_{spr} (1354 °C) < U_{spr} (1400 °C) < U_{spr} (1450 °C) ≤ U_{spr} (1500 °C), as shown in Fig. 4a.

The contact angle of the Si-10Zr/GC system was measured at T = 1400 °C in t = 45 s and the value of $\theta = 55°$ was obtained. The same value was found in t = 30 s at T = 1450 °C.

As shown in Fig. 4b where the wetting kinetics observed within the first 150 s are displayed, the further decrease in the contact angles to their equilibrium values occurred in 60 s ($\theta = 51 \div 52°$), 15 s ($\theta = 49°$) and 8 s ($\theta = 43°$) at the Si-10Zr/GC interfaces at T = 1354, 1400 and 1450 °C, respectively.

The wetting experiment performed at T = 1500 °C deserves a more detailed discussion. As abovementioned, the spreading kinetics observed at the Si-10Zr/GC interfaces at T = 1450 °C and T = 1500 °C are almost overlapped. It might be given by a delay exhibited by the alloy drop processed at T = 1500 °C in achieving the same heating rate imposed by the experimental device. Contrarily, the effect of the different testing temperatures is strongly evinced by analyzing the equilibrium contact angle values measured at the Si-10Zr/GC interfaces after 15 min: $\theta = 43°$ and $\theta = 40°$, at T = 1450 °C and T = 1500 °C, respectively.

BSE/EDS analyses performed at the top drop and at the triple line of the Si-10Zr/GC sample processed at T = 1354 °C for 15 min,

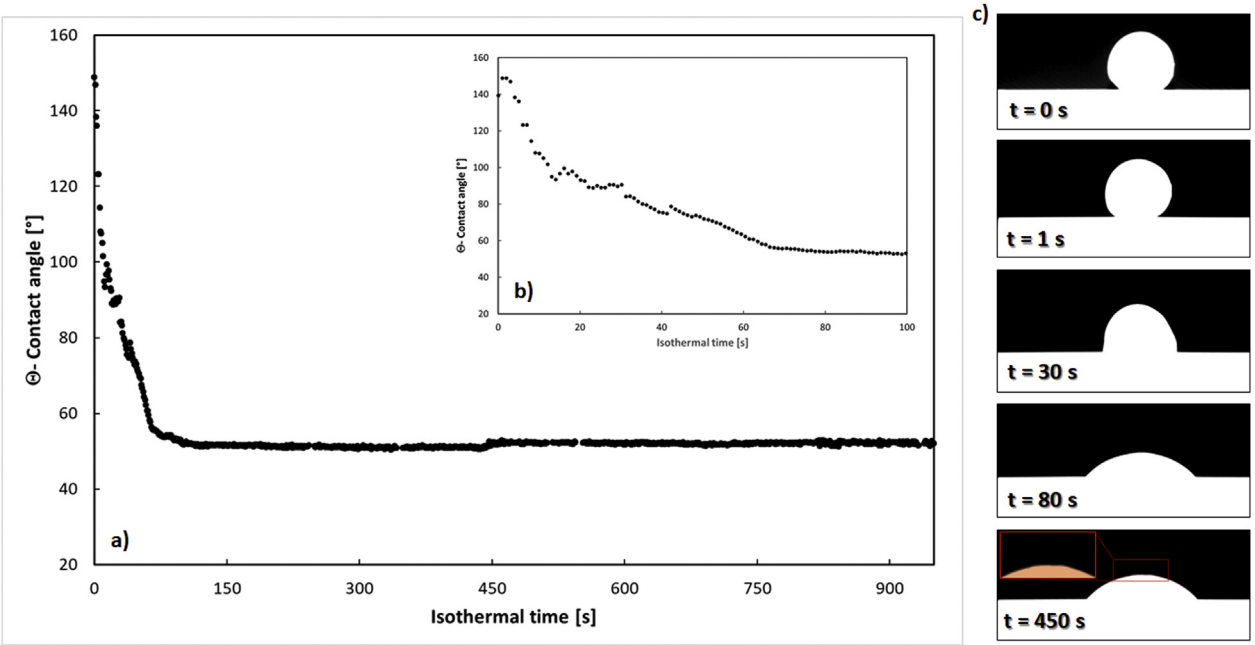

Fig. 3. Wettability of the Si-10Zr/GC couple at T = 1354 °C for 15 min under an Ar atmosphere: a) and b) contact angle behaviors as a function of time and c) time sequence images recorded during the wetting test.

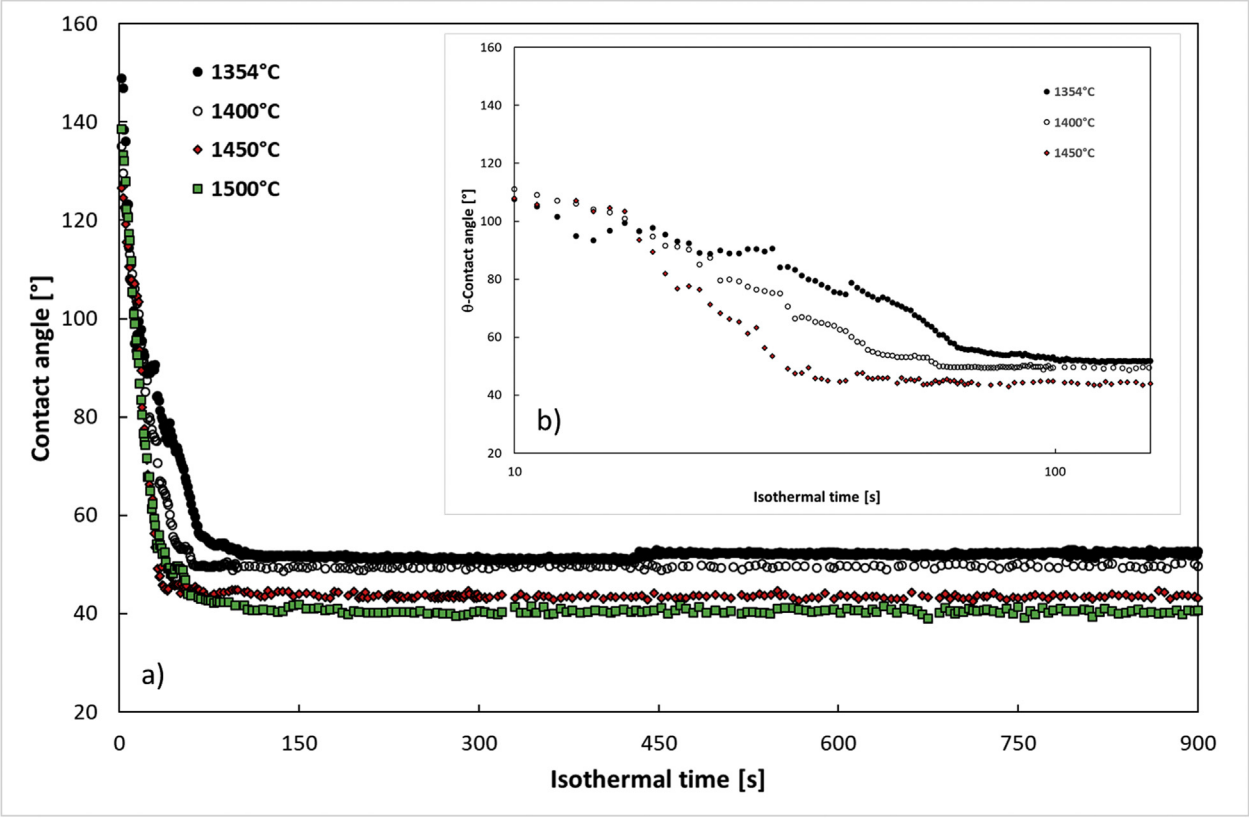

Fig. 4. Wettability of the Si-10Zr/GC couples for 15 min under an Ar atmosphere at: (●) T = 1354 °C; (○) T = 1400 °C; (◆) T = 1450 °C and (■) T = 1500 °C.

are shown in Fig. 5. As it can be seen, at the top of the solidified drop, $ZrSi_2$ as segregated phase was detected (Fig. 5 a). On the other hand, a "shadow" surrounding the drop perimeter at the triple line is revealed (Fig. 5 b and c). In particular, several SiC crystals close to the Si-Zr alloy drop triple line are detected. In addition, moving far from the triple line, unreacted regions of GC with over-layered circular and narrowing areas of SiC are found. Due to fast cooling of the sample at the end of the wetting experiment, a crack at the interface was observed.

Similarly, at the interface of the alloy samples processed at higher temperatures, the same "shadow" and the crack were observed, as shown in Fig. 6.

The crack at the interface was most probably caused by the mismatch in the thermal expansion coefficients and by the strong adherence of Si-Zr alloy at the SiC layer. The "shadow" consists of a thin SiC layer grown beyond the triple line and it is clearly influenced by the temperature, associated with vaporization/condensation phenomena. The GC circular area surrounding the alloy drop was completely covered by the thin SiC layer and its radius is temperature dependent. It seems that the thickness of the SiC layer and its morphology are also influenced by temperature. As already observed for the sample processed at the lowest temperature, circular and narrowing areas of SiC with a radius inversely proportional to the distance from the triple line are noticed. Moreover, as it can be seen in the Fig. 6d) and e) and f) the presence of SiC crystals grown up at the triple lines with a size correlated to the testing temperature are detected.

At the Si-10Zr/GC interface, a SiC layer as unique reaction product with different microstructural evolution was detected (Fig. 7). In particular, the crossed-sectioned Si-10Zr/GC samples processed at T = 1354 °C and T = 1500 °C for 15 min are shown (Fig. 7a–b). After the wetting test performed at T = 1354 °C, at the triple line of the Si-10Zr/GC sample, SiC crystals epitaxially grown up to a size of 2 ÷ 7 μm as well as the presence of C-dissolution

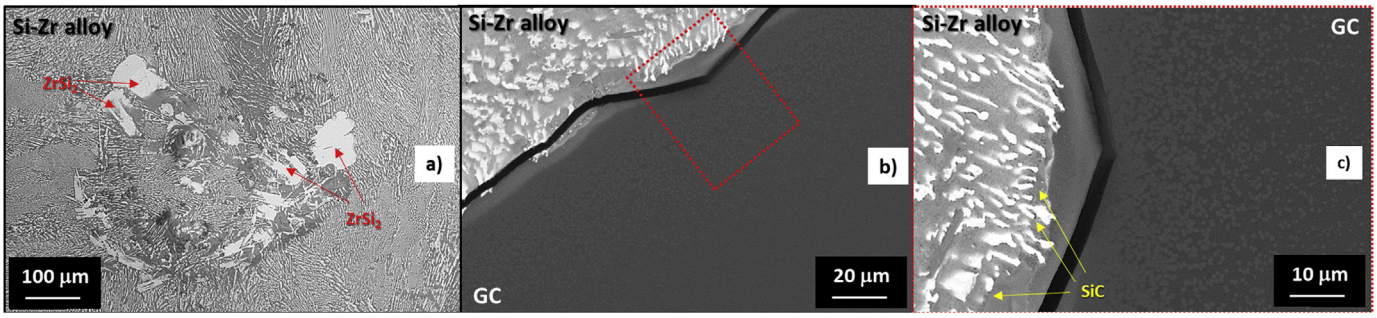

Fig. 5. BSE/EDS analyses performed on the Si-10Zr/GC sample after the wetting test at T = 1354 °C: a) top of the solidified drop; b) and c) triple line at two different magnifications.

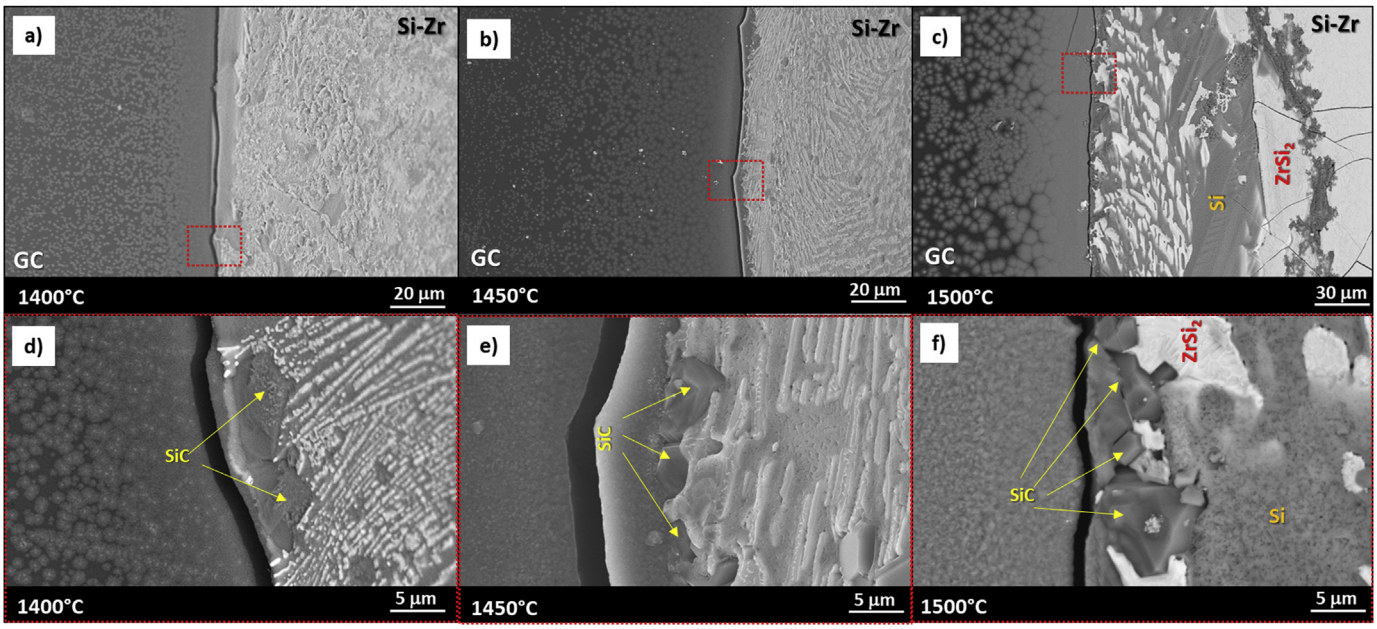

Fig. 6. BSE/EDS analyses performed at two different magnifications at the triple line of the Si-10Zr/GC samples after the wetting tests performed at: a) and d) T = 1400 °C; b) and e) T = 1450 °C; c) and f) T = 1500 °C.

pockets, were detected (Fig. 7c). The same type of microstructure was found in the middle of the drop (Fig. 7e). Moreover, at higher magnification is possible to identify easily the interface formed at the initial stage of the reaction with the C-dissolution pockets at the bottom, a two phase of $ZrSi_2$+SiC inside, and at the top of the interface, close to the alloy, the SiC crystals with a size varying from 0.5 to 5 μm. Contrarily, both near and far from the triple line (middle of the drop) of the Si-10Zr/GC sample processed at T = 1500 °C, a compact layer generated by the packing of SiC crystals epitaxially grown up to 10 μm was detected (Fig. 7d–f). In both cases, the solidified alloy drop exhibits a Si-$ZrSi_2$ two-phase microstructure. In particular, needle shaped $ZrSi_2$ crystals embedded in a Si-matrix were found.

3.2. Wettability by the contact-heating sessile drop method as a function of time

In Fig. 8, the contact angle values displayed by the liquid Si-10Zr alloys in contact with GC at T = 1450 °C for 15 min and 45 min, are shown. As expected, almost the same kinetics of spreading exhibited by the two couples is observed, as shown in Fig. 8b.

It is worth to highlight that such outcome may be useful in establishing the reliability of both the results obtained and the procedure applied.

In both cases, the steady state equilibrium contact angle was achieved in 40 s after the melting of the alloy drops and, after 15 min, the same contact angle value of $\theta = 43°$ was measured. On the other hand, a slight increase in the contact angle up to $\theta = 45°$ was shown by the liquid alloy in contact with the GC substrate after 45 min.

As it can be seen in Fig. 9, a compact layer of SiC is detected at both the triple lines (Fig. 9a and b). However, for the sample processed for 15 min, a homogeneous SiC layer with a thickness of 4 ÷ 5 μm was detected. On the contrary, increasing three times the duration of the experiment, an irregular SiC layer with a thickness around 4 ÷ 12 μm, was revealed. In addition, at the triple lines, few C-dissolution pockets were still present.

Moving in the middle of the drop, different microstructures were detected, as shown in Fig. 9c–d. Indeed, at the Si-10Zr/GC interface, processed for 15 min, an alternating microstructure of packed and un-packed SiC crystals was found, generating compact and less compact reaction layers in contact with the Si-Zr alloy. In the latter case, at the interface formed during the initial stage of the reaction, individual SiC crystals with a size of about 5 μm and C-dissolution pockets were detected. By tripling the time of contact with the GC substrate, the appearance of a more compact SiC layer with an average thickness of 5 μm even far from the triple line is promoted (Fig. 9d).

4. Discussion

The experimental results of the contact angles and average thicknesses of SiC reaction layers formed during the wetting tests as functions of operating conditions are collected in Table 1.

Various eutectic compositions in the Si-rich side of the Si-Zr system and temperatures differing up to 30 °C with respect to the eutectic melting temperature range, are reported in Refs. [40,41]. In particular, the analysis of the invariant reactions in the Si-Zr system indicates the Si-10Zr alloy as the eutectic one [16,17] with a melting range of 1355.15 ÷ 1370 °C.

In this work, the melting temperature of the Si-10Zr alloy was detected at T = 1354 °C, is in a very good agreement with literature data [17]. However, as evidenced by the EDS analyses performed on as-produced cross-sectioned alloy sample (Fig. 1), a two-phase microstructure, typical of hypoeutectic alloys, was revealed. In particular, $ZrSi_2$ phase was rejected during the solidification as a segregating phase at the surface and embedded at the bottom of the drop in an eutectic matrix with a content of Zr varying from 8.1 to 9 at%. Indeed, in the Si-rich part of the Si-Zr system, the last re-assessment of the Si-Zr phase diagram [41] indicates the eutectic composition of Si-8.19Zr at T = 1345.7 °C.

During the wetting test performed at T = 1354 °C, the melting of the alloy was even promoted and the liquid state preserved by the occurring exothermic reaction at the alloy/GC interface between Si and C [43]:

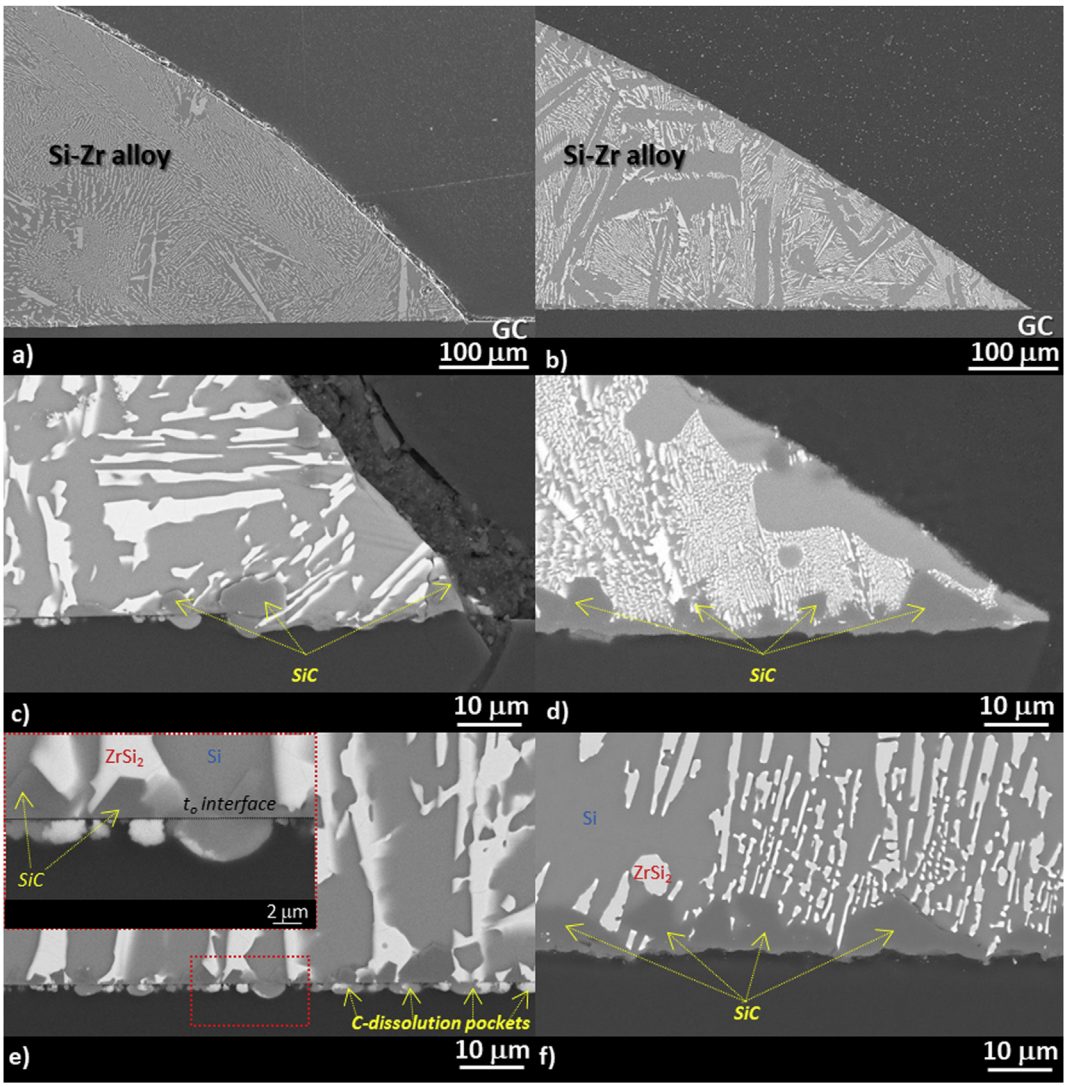

Fig. 7. BSE/EDS analyses performed at three different magnifications at the cross-sectioned Si-10Zr/GC samples after the wetting tests performed at: T = 1354 °C a), c) near the triple line and e) far from the triple line; T = 1500 °C b), d) near the triple line and f) far from the triple line.

$$Si_{(l)} + C_{(s)} \rightarrow SiC_{(s)} \quad (1)$$

However, the presence of a SiO_2-native oxide layer at the alloy surface, usually found during the wetting tests performed by the contact heating sessile drop [31], may delay to reach the complete melting of the drop. Nevertheless, the native oxide should be decomposed by the reaction (2) with the underlying liquid Si, forming the volatile Si monoxide [43]:

$$SiO_{2(s)} + Si_{(l)} \rightarrow 2SiO_{(g)} \uparrow \quad (2)$$

When the layer of native oxide completely disappears at the interface, liquid Si is able to interact with the substrate.

Analyzing the spreading behavior of the Si-Zr alloy on GC following the evolution of the drop radius over time (R), three different stages with three different spreading rates can be identified, as shown in Fig. 10. At the Si-10Zr/GC triple line, the contact angle value decreased from approximately 149°–110° within the first 15 s ($t_0 < t < t_1$) and a linear spreading behavior was observed ($U_{spread} \approx 25$ μm/s). During this stage, a strong reaction (1) between liquid Si and C at the interface occurred. Indeed, linear spreading behaviors are associated to the reactive wetting [43,44].

In the next 65 s ($t_1 < t < t_2$), a decrease in the slope of the spreading curve over time was observed ($U_{spread} \approx 15$ μm/s) and the Si-10Zr alloy started to "wet" GC substrate with the contact angle value decreased down to about $\theta = 55°$.

It worth to be pointed out that liquid Si and Si-based alloys do not wet but strongly react with C by means of the reaction (1). Actually, the wettable substrate is SiC, which is already present at the interface as the reaction product defined by (1).

In the third stage ($t_2 < t < t_3$) approaching the steady state condition (with an equilibrium contact angle of about $\theta = 51 \div 52°$), a decrease of 10 times in the slope of the spreading curve was observed.

Additionally, the appearance of SiC crystals growing at the interface, mainly at the triple line (Fig. 7), may reduce the wettability (by increased roughness). Within this last stage, a further advancing of the triple line can be promoted by evaporation and condensation phenomena of Si beyond the drop perimeter.

After 450 s, with the appearance of $ZrSi_2$ solid phase at the top of the drop, a slight increase (i.e. dewetting) in the contact angle was observed (Figs. 3c and 5a). Most probably, the interaction between the alloy and C-substrate within the first 450 s resulted in a

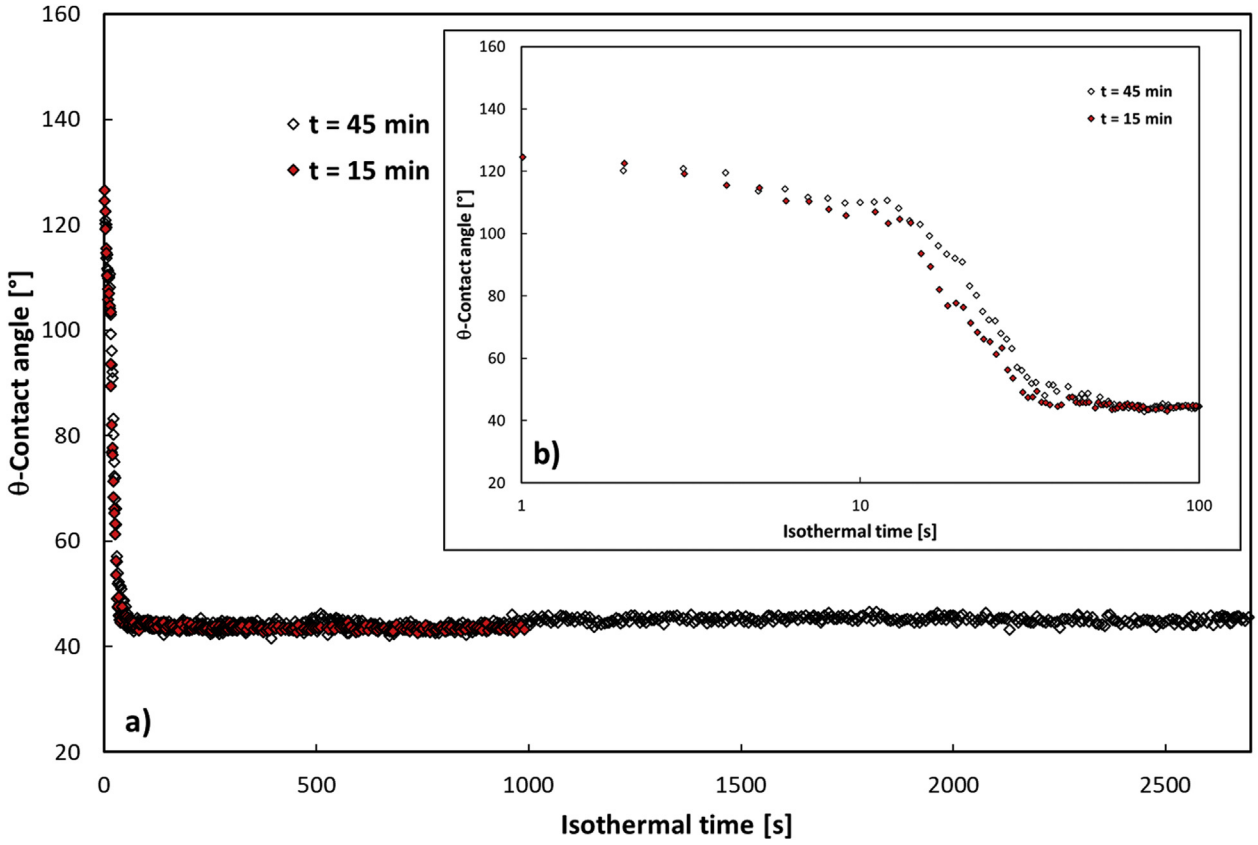

Fig. 8. Evolution of contact angle values of Si-10Zr/GC couples after the wetting tests performed at T = 1450 °C for: a) 900 s (15 min) and b) the first 100 s.

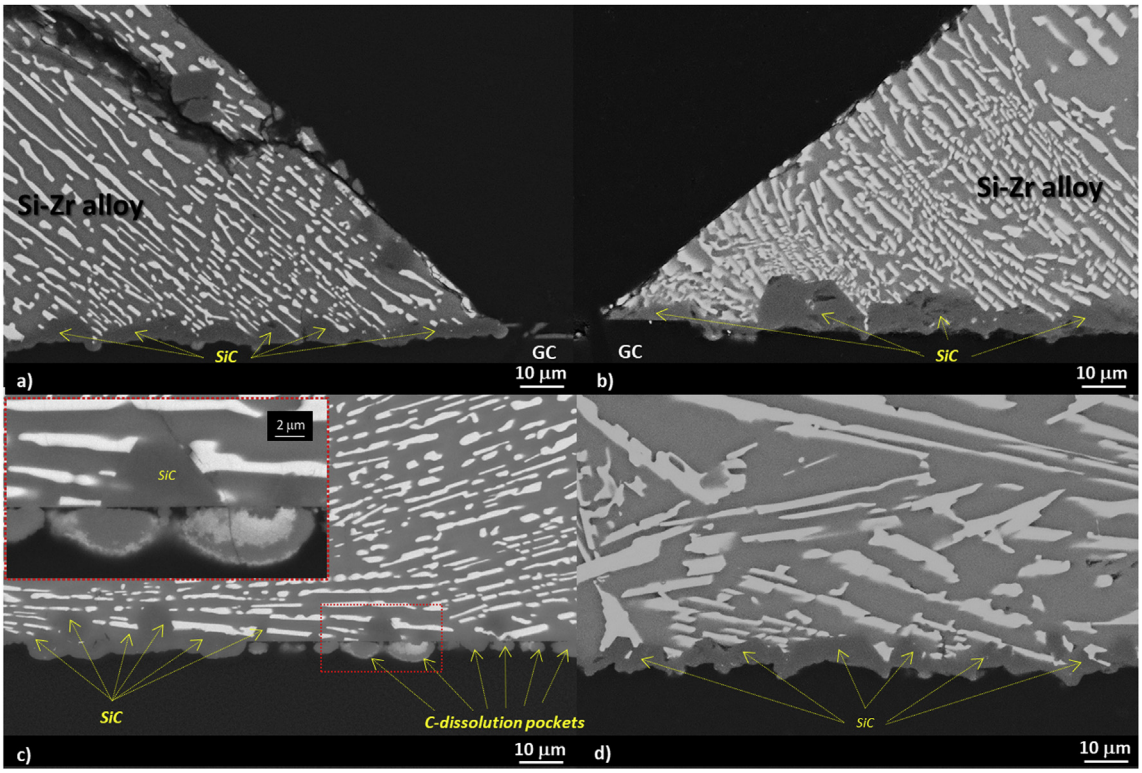

Fig. 9. BSE/EDS analyses performed near and far from the triple lines of the cross-sectioned Si-10Zr/GC samples after the wetting test at T = 1450 °C for: 15 min a) and c); 45 min b) and d).

Table 1
Contact angle values and SiC-layer average thickness both at the triple lines (TL) and in the middle of the drop (MD) as functions of temperature and time.

Temperature [°C]	time [min]	θ_f [°]	SiC-thickness [μm] TL	SiC-thickness [μm] MD
1354	15	51 ÷ 52	4.5	5
1400	15	49	5	5
1450	15	43	4.5	5
1450	45	45	8	5
1500	15	40	6	6

displacement of the alloy composition (with an increased melting temperature) as a consequence of a decrease in Si-content. Accordingly, further C-dissolution and epitaxial growth of SiC crystals were probably suppressed or even impeded.

Concerning the kinetics of spreading, all the interaction phenomena, i.e. the reaction, C-dissolution, growth of SiC at the interface, mainly at the triple line, are enhanced with an increase in temperature (see Table 1). Indeed, as shown in the insert of the Fig. 4, the spreading rate increased with temperature. In particular, at T = 1450 °C and T = 1500 °C, only two spreading regimes were found. It let us to conclude that the kinetics of SiC crystals growth and, in particular, their packaging at the triple line are more favored at higher temperatures (Fig. 7). Consequently, an equilibrium contact angle is reached faster than at the lower temperatures.

As aforementioned, the evaporation/condensation phenomena at higher temperatures are more pronounced and may contribute to the advancing triple line, therefore a decrease in the contact angle may be observed (Figs. 4 and 6, Table 1).

The growth followed by the packaging of SiC crystals are greatly influenced by time (Fig. 9), where at the Si-10Zr/GC interface, after 45 min, almost double thickness with respect to that of a short-term experiment was observed. An increase in the contact angle value may be explained by higher surface roughness (Table 1).

Under equilibrium conditions, a multi-step mechanism can be identified, resulting in the evolution of interface microstructure, is shown in Fig. 11.

In agreement with [45], in the first instance of contact between liquid silicon and carbon, at the alloy/GC interface, by means of (1), a very thin quasi-continuous (fragmented) layer is formed (Fig. 11a and b). In parallel, the dissolution of C is promoted by the presence of open channels along the thin SiC layer (Fig. 11c). Being Si and C in contact, the C-dissolution generates the formation of cavities (namely C- dissolution pockets), which are filled by the liquid alloy. The diffusion between the liquid alloy and GC substrate, favours the appearance of SiC crystals epitaxially grown over time (1 < t < 15, in min) close to the C-dissolution pocket (Fig. 11d).

Under equilibrium conditions, the aforementioned phenomena are strongly influenced by the temperature. In fact, BSE images of the Si-10Zr samples processed at T = 1354 °C and T = 1450 °C, respectively, are shown in Figs. 7e and 9c. The presence of a compact SiC layer alternated with individual SiC crystals above the C-dissolution pockets were detected. On the contrary, at T = 1500 °C in 15 min, the microstructure developed at the interface shows an compact SiC layer resulting from the packaging of SiC crystals on the interface at the initial stage of reaction and further formation of SiC by the reaction of the Si-Zr alloy with the remaining C inside the dissolution pockets (Fig. 11e). For the Si-10Zr/GC system, at T = 1450 °C in t > 15 min, this phenomenon is identified as the last stage of SiC layer growth, as shown in Fig. 9d. Additionally, for t ≥ 15 min, parallel SiC dissolution and re-precipitation over SiC crystals may contribute to the further growth of the SiC crystals at the interface and their packaging results in a more compact and thicker SiC discontinuous layer (Fig. 11f). Such fragmentation allows the Si-Zr alloy to be again in direct contact with unreacted C by dissolving SiC thin layer and then, between two SiC compacted fragments, a new C-dissolution pocket is formed (Fig. 11g and h).

Despite the affinity of the both alloy components for C [46,47] to produce stable ZrC and SiC (Gibbs free energies of formation: $\Delta G^\circ_{f\ TiC} = -300$ kcal/mol and $\Delta G^\circ_{f\ SiC} = -147$ kcal/mol), concerning the alloy composition with a Zr-content equal to 10 at% together with the operating conditions applied in this study, the interfacial

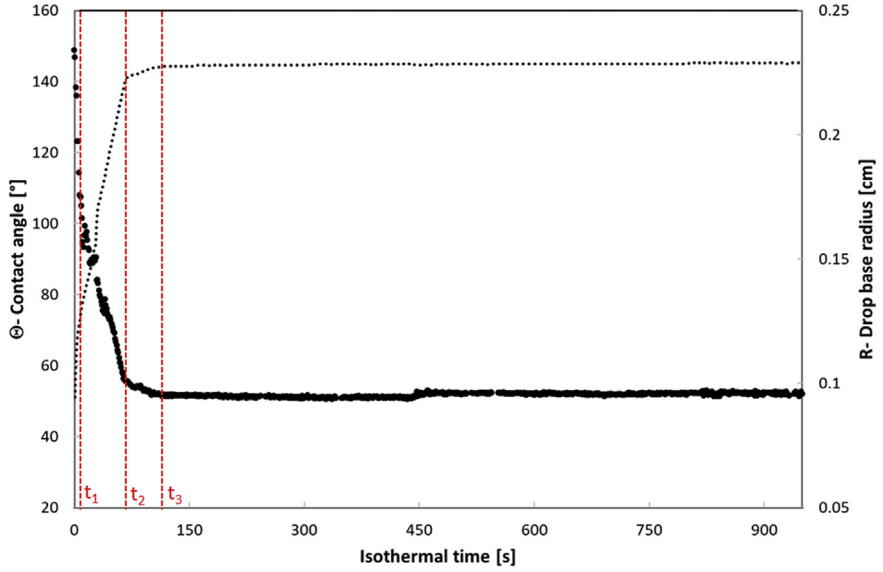

Fig. 10. Evolution of the contact angle values (●) and R-drop base radius (—) over time of Si-10Zr/GC observed within the wetting test at T = 1354 °C for 15 min.

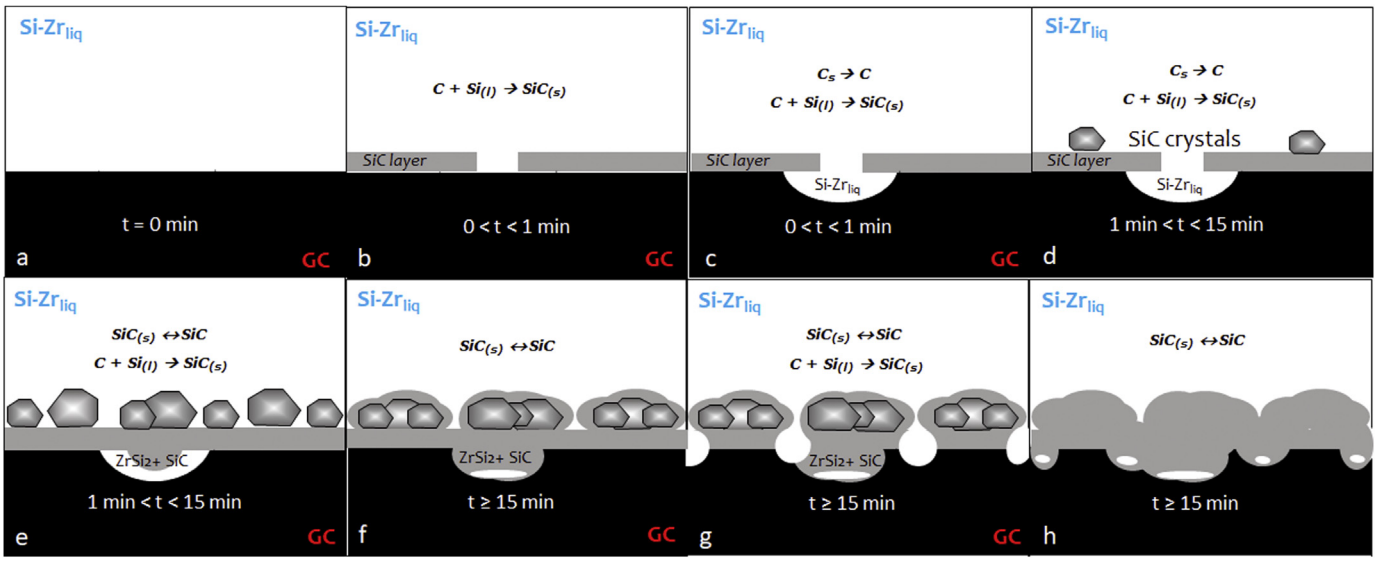

Fig. 11. Schematic of all the possible interfacial phenomena occurring at the Si-10Zr/GC interface and a)-h) their evolution in time.

reaction of liquid Si to produce SiC is thermodynamically more favored with respect to the formation of ZrC [42] as confirmed by EDS analyses performed at the interfaces (Figs. 7 and 9).

Moreover, it is well known that liquid Si and Zr react with oxygen forming the oxides for the temperature range investigated. However, oxidation and oxygen transport phenomena at the alloy surface can be neglected if the presence of counter flows of volatile mono-oxides SiO is taken into account, as demonstrated by Refs. [48,49]. The appearance of stable oxides at the surface is further suppressed by the high evaporation tendency of liquid Si [30,31,46]. In fact, condensed Si and Si-oxide fogs might be present in the gas phase surrounding the drop, acting as a barrier and suppressing the O_2-flow coming from the atmosphere to the alloy surface [49]. Such phenomenon can explain the growth of circular area of SiC detected far from the triple line (Figs. 5 and 6). However, as already reported in Ref. [31], the pronounced evaporation observed at the Si-10Zr/GC triple lines with the formation of a thin reaction layer surrounding the drop perimeter, seems to not promoting further contact angle advancement as contrarily observed for Si-Co eutectic alloy/GC [32]. It may be explained by different thermophysical properties of the two liquid systems which probably allow a higher stability of the Si-Zr alloy respect to the Si-Co eutectics [50].

The equilibrium contact angle values measured at Si-10Zr/GC triple line as a function of the temperature are comparable with the values measured for Si-8Zr/GC system under an Ar atmosphere [38]. In particular, the contact angle value measured at Si-8Zr/GC interface is weakly influenced by an increase in temperature from 1404 °C (detected melting point) to 1450 °C. Indeed, during the heating of the sample, the contact angle increased from 44° to 45°. This can be attributed to the growth of SiC crystals at the interface and consequently an increased roughness of the surface. In addition, as demonstrated in this work, the size of SiC crystals grown at the interface is influenced by the both operating parameters, i.e. the temperature and time. Furthermore, the contact angle measurements [38] were performed under dynamic conditions in a unique experiment and the wettability could be affected by the interfacial phenomena such as thickening of SiC layer already occurred at lower temperatures.

5. Conclusions

Wettability and reactivity studies of liquid Si-10Zr alloy in contact with GC were performed by the contact heating sessile drop method as a function of temperature and time under an atmosphere with reduced oxygen content.

The interfacial phenomena observed in the present study, i.e. the contact angle behaviors, spreading kinetics, microstructural evolution, were analysed, discussed and related to the operating conditions. The final contact angle values measured at the Si-10Zr/GC interfaces over the temperature range of T = 1354–1500 °C, were decreased from 52° to 40°.

At higher temperatures, the enhanced growth of the interfacial layer, mainly at the triple line as well as Si-evaporation/condensation phenomena were observed.

In particular, the results obtained indicate that the wettability and spreading kinetics of the Si-Zr alloy on GC, observed at the interface and at the triple line are controlled by the growing and thickening of SiC crystals, detected as a unique reaction product.

A careful investigation at T = 1450 °C which is the temperature usually selected to produce advanced composites by reactive melt infiltration process was performed. The growth and thickening of SiC at the interface are time-dependent.

Taking into account the interfacial phenomena, the contact angle values measured at the Si-10Zr/GC interface are comparable and in a very good agreement with literature data.

The results obtained can be helpful to identify the key parameters affecting the manufacturing of SiC/$ZrSi_2$ and C/C-ZrC-SiC composite materials. In this context, the interfacial phenomena related to the liquid Si-Zr alloy/SiC system should be evaluated. Additionally, to optimize reactive infiltration process, the understanding of pore closure/narrowing phenomena and the reactivity as a function of Si-content is worthy to be investigated, as well as the thermophysical properties such as the surface tension and viscosity, which can be used as input data for modelling.

Author contribution section

- Donatella Giuranno: Investigation, Formal analysis, Conceptualization, Writing - original draft, Writing – review & editing.

- Adelajda Polkowska: Microstructural Characterization
- Wojciech Polkowski: Formal Analysis, Conceptualization, Writing.
- Rada Novakovic: Supervision, Formal analysis, Writing – review & editing Conceptualization.

Acknowledgments

The NCN-National Science Center, Poland is greatly acknowledged for the financial support through the POLONEZ project number UMO-2016/23/P/ST8/01916. This project was carried out under POLONEZ-3 program which has received funding from European Union's Horizon 2020 research and innovation program under Marie Skłodowska-Curie grant agreement. No 665778

.

References

[1] D.B. Miracle, Aeronautical applications of metal-matrix composites, in: S.D. Henry, et al. (Eds.), ASM Handbook, ASM International, Ohio, USA, 2001.
[2] X. Zhang, Y. Chen, J. Hu, Recent advances in the development of aerospace materials, Prog. Aerosp. Sci. 97 (2018) 22–34.
[3] H. Singh, S.J. Nrip, A.K. Tyagi, An overview of metal matrix composite: processing and SiC based mechanical properties, J. Eng. Res. Stud. 2 (4) (2011) 72–78.
[4] M. Rosso, Ceramic and metal matrix composites: routes and properties, J. Mater. Process. Technol. 175 (2006) 364–375.
[5] E.P. Simonenko, D.V. Sevastyanov, N.P. Simonenko, V.G. Sevastyanov, N.T. Kuznetsov, Promising Ultra_High_Temperature ceramic materials for aerospace applications, Russ. J. Inorg. Chem. 58 (14) (2013) 1669–1693.
[6] S.T. Mileiko, Constituent compatibility and microstructural stability, Compr. Compos. Mater. 4 (2000) 265–287.
[7] A. Siddharth Sharma, P. Fitriani, D.H. Yoon, Fabrication of SiCf/SiC and integrated assemblies for nuclear reactor applications, Ceram. Int. 43 (2017) 17211–17215.
[8] T. Koyanagi, Y. Katoh, T. Nozawa, L.L. Snead, S. Kondo, C.H. Henager Jr., M. Ferraris, T. Hinoki, Q. Huang, Recent progress in the development of SiC composites for nuclear fusion applications, J. Nucl. Mater. 511 (2018) 544–555.
[9] M. Li, X. Zhou, H. Yang, S. Du, Q. Huang, The critical issues of SiC materials for future nuclear systems, Scr. Mater. 143 (2018) 149–153.
[10] Y.G. Tong, Z.H. Cai, S.X. Bai, Y.L. Hu, M.Y. Hua, W. Xie, Y.C. Ye, Y. Li, Microstructures and properties of Si-Zr alloy based CMCs reinforced by various porous C/C performs, Ceram. Int. 44 (2018) 16577–16582.
[11] Z. Zhou, Z. Sun, Ge Yicheng, Ke Peng, Ran Liping, Yi Maozhong, Microstructure and ablation performance of SiC–ZrC coated C/C composites prepared by reactive melt infiltration, Ceram. Int. 44 (2018) 8314–8321.
[12] Y. Katoh, L.L. Snead, C.H. Henager Jr., A. Hasegawa, A. Kohyama, B. Riccardi, H. Hegeman, Current status and critical issues for development of SiC composites for fusion applications, J. Nucl. Mater. 367–370 (2007) 659–671.
[13] S.P. Murarka, Transition metal silicides, Annu. Rev. Mater. Sci. 13 (1983) 117–137.
[14] Kyung-Tae Park Il-Je Cho, Sang-Ki Lee, Hayk H. Nersisyan, Yong-Soo Kim, Jong-Hyeon Lee, Rapid and cost-effective method for synthesizing zirconium silicides, Chem. Eng. J. 165 (2010) 728–734.
[15] M. Le Flem, J. Canel, S. Urvoy, Processing and characterization of Zr3Si2 for nuclear applications, J. Alloy. Comp. 465 (2008) 269–273.
[16] H. Okamota, Bull. Alloy Phase Diag. 11 (5) (1990) 513–519.
[17] C. Gueneau, C. Servant, I. Ansara, N. Dupin, Thermodynamic assessment of the Si-Zr system, Calphad 18 (3) (1994) 319–327.
[18] C. Colinet, R. Viennois, J.C. Tedenac, First principles study of the structural stability of intermetallic compounds in the Si–Zr system, Calphad Comput. Coupling Phase Diagrams Thermochem. 36 (2012) 118–126.
[19] H. Yeom, L. He, R. Mariani, K. Sridharan, Structural evolution of oxidized surface of zirconium-silicide under ion irradiation, Appl. Surf. Sci. 455 (2018) 333–342.
[20] S. Tkachenko, O. Datskevich, L. Kulak, H. Engqvist, C. Persson, Tribological properties of Ti-Si-Zr alloys, in: Metal 2013 Conference, 15-17.5, 2013 (Brno, Czech Republic).
[21] C. Li, Y. Zhan, W. Jiang, Zr–Si biomaterials with high strength and low elastic modulus, Mater. Des. 32 (2011) 4598–4602.
[22] J. Jiang, S. Wang, W. Li, Z. Chen, Fabrication of Cf/ZrC–SiC composites using Zr–8.8Si alloy by melt infiltration, Ceram. Int. 41 (2015) 8488–8493.
[23] Y. Tong, S. Bai, Y. Hu, X. Liang, Y. Ye, Q.H. Qin, Laser ablation resistance and mechanism of Si-Zr alloyed melt infiltrated C/C-SiC composite, Ceram. Int. 44 (2018) 3692–3698.
[24] O.C. Esteban, M. Caccia, A. Camarano, J. Narciso, Advances in High Temperature Ceramic Matrix Composites and Materials for Sustainable Development; Ceramic Transactions, John Wiley & Sons, 2017.
[25] A.J. Whitehead, T.F. Page, Fabrication and characterization of some novel reaction-bonded silicon carbide materials, J. Mater. Sci. 27 (1992) 839–852.
[26] M. Caccia, J. Narciso, Key parameters in the manufacture of SiC-based composite materials by reactive melt infiltration, Materials 12 (15) (2019) 2425.
[27] R. Novakovic, D. Giuranno, M. Caccia, S. Amore, R. Nowak, N. Sobczak, J. Narciso, E. Ricci, Thermodynamic, surface and structural properties of liquid Co-Si alloys, J. Mol. Liq. 221 (2016) 346–353.
[28] R. Novakovic, S. Amore, D. Giuranno, E. Ricci, R. Nowak, N. Sobczak, Thermodynamic and surface properties of liquid Ge-Si alloys, Calphad Comput. Coupling Phase Diagrams Thermochem. 44 (2014) 95–101.
[29] D. Giuranno, A. Tuissi, R. Novakovic, E. Ricci, Surface tension and density of Al-Ni alloys, J. Chem. Eng. Data 55 (2010) 3024–3028.
[30] D. Giuranno, N. Sobczak, G. Bruzda, R. Nowak, W. Polkowski, A. Kudyba, A. Polkowska, R. Novakovic, Studying the wettability and reactivity of liquid Si-Ti eutectic alloy on glassy carbon, J. Mater. Eng. Perform. 28 (6) (2019) 3460–3467.
[31] D. Giuranno, N. Sobczak, G. Bruzda, R. Nowak, W. Polkowski, A. Kudyba, A. Polkowska, R. Novakovic, Wetting and spreading behavior of liquid Si-Ti eutectic alloy in contact with glassy carbon and SiC at T = 1450 °C, Metall. Mater. Trans. A (2019), https://doi.org/10.1007/s11661-019-05382-y.
[32] M. Caccia, S. Amore, D. Giuranno, R. Novakovic, E. Ricci, J. Narciso, Towards optimization of SiC/$CoSi_2$ composite material manufacture via reactive infiltration: wetting study of Si–Co alloys on carbon materials, J. Eur. Ceram. Soc. 35 (15) (2015) 4099–4106.
[33] R. Voytovych, V. Bougiouri, N.R. Calderon, J. Narciso, N. Eustathopoulos, Reactive infiltration of porous graphite by NiSi alloys, Acta Mater. 56 (2008) 2237–2246.
[34] J. Roger, G. Chollon, Mechanisms and kinetics during reactive infiltration of molten silicon in porous graphite, Ceram. Int. 45 (2019) 8690–8699.
[35] E. Louis, J.A. Miralles, J.M. Molina, Reactive infiltration: identifying the role of chemical reactions, capillarity, viscosity and gravity, J. Mater. Sci. 52 (2017) 7530–7538.
[36] Y. Tong, H. Zhang, X.B. Liang, C.Y. Lee, S.X. Bai, Q.H. Qin, Surface tension calculation of Si-Zr alloys for reactive infiltration of SiC and/or ZrC based ceramic composites, Res. Rev. Mater. Sci. Chem. 6 (2) (2016) 115–130.
[37] B.J. Keene, A review of the surface tension of Silicon and its alloys with reference to Marangoni Flow, Surf. Interface Anal. 10 (1987) 367–383.
[38] M. Naikadea, B. Fankhänel, L. Weber, A. Ortona, M. Stelter, T. Graule, Studying the wettability of Si and eutectic Si-Zr alloy on carbon and silicon carbide by sessile drop experiments, J. Eur. Ceram. Soc. 39 (2019) 735–742.
[39] L. Liggieri, A. Passerone, An automatic technique for measuring the surface tension of liquid metals, High Technol. 7 (1989) 80–86.
[40] N. Eustathopoulos, N. Sobczak, A. Passerone, K. Nogi, Measurement of contact angle and work of adhesion at high temperature, J. Mater. Sci. 40 (2005) 2271–2280.
[41] H.M. Chen, F. Zheng, H.S. Liu, L.B. Liu, Z.P. Jin, Thermodynamic assessment of B–Zr and Si–Zr binary systems, J. Alloy. Comp. 468 (2009) 209–216.
[42] H.M. Chen, Y. Xiang, S. Wang, F. Zheng, L.B. Liu, Z.P. Jin, Thermodynamic assessment of the C–Si–Zr system, J. Alloy. Comp. 474 (2009) 76–80.
[43] B. Drevet, N. Eustathopoulos, Wetting of ceramics by molten silicon and silicon alloys: a review, J. Mater. Sci. 47 (2012) 8247–8260.
[44] O. Dezellus, F. Hodaj, N. Eustathopoulos, Chemical reaction-limited spreading: the triple line velocity versus contact angle relation, Acta Mater. 50 (2002) 4741–4753.
[45] R. Voytovych, R. Israel, N. Calderon, F. Hodaj, N. Eustathopoulos, Reactivity between liquid Si or Si alloys and graphite, J. Eur. Ceram. Soc. 32 (14) (2012) 3825–3835.
[46] O. Knacke, O. Kubashewski, K. Hesselmann, Thermochemical Properties of Inorganic Substances, second ed., Springer Verlag, Düsseldorf, 1991.
[47] T.B. Massalski, Binary Alloy Phase Diagrams, s. 1, ASM, Metals Park, OH, 1986, p. 2.
[48] D. Giuranno, E. Arato, E. Ricci, Oxidation conditions of pure liquid metals and alloys, Chem. Eng. Trans. 24 (2011) 571–576.
[49] M. Ratto, E. Ricci, E. Arato, Mechanism of oxidation/deoxidation of liquid silicon: theoretical analysis and interpretation of experimental surface tension data, J. Cryst. Growth 217 (3) (2000) 233–249.
[50] T. Iida, R.I.L. Guthrie, The Physical Properties of Liquid Metals, Clarendon Press, Oxford, 1993.